

Investigation of Sequential and Simultaneous Crossflow Heat Exchangers for Automotive Application

Mohammed Ismail¹, Mesbah G. Khan², Amir Fartaj¹

¹University of Windsor

401 Sunset Avenue, Windsor, Ontario, Canada
ismailf@uwindsor.ca; fartaj@uwindsor.ca

²Sanden International (U.S.A.) Inc.

47772 Halyard Drive, Plymouth, MI, U.S.A.
khan13j@uwindsor.ca

Abstract - In current research, forced convective heat transfer of sequential and simultaneous heat exchangers are numerically investigated. Both, the sequential and the simultaneous, modules of heat exchangers are identical in size, i.e. frontal area and volume. The simulations have been conducted on serpentine finned heat exchangers in air-to-liquid cross-flow orientation using ANSYS FLUENT, a widely used finite volume method (FVM) commercial code. The heat transfer are concurrently obtained for automatic transmission fluid (ATF) and 50% ethylene glycol-water mixture (EG). In the airside, the constant inlet temperature and velocity of the air have been maintained at 25⁰C and 6.3 m/s respectively. In liquid side, the inlet temperature of ATF and EG have also been kept constant at 150⁰C and 105⁰C respectively. For both the sequential and the simultaneous orientations, air has been used to cool ATF and EG at various massflow rates within a laminar flow regime. For a given Reynolds number, simultaneous heat exchanger module displays significant enhancement of heat transfer rate than that of the conventional sequential module.

Keywords: Automatic transmission fluid, glycol-water mixture, numerical, laminar flow, crossflow, simultaneous, sequential, heat transfer.

1. Introduction

Heat is one of the most important forms of energy that has versatile applications in domestic, commercial, transportation and industrial sectors on a daily basis. Energy demands in every sector have been increasing progressively, while the energy sources are limited [1]. For that reason, it is the paramount for many industries to develop such a heat transfer device that can deliver higher heat transfer. In order to mitigate increasing energy demands, researchers [2], [3]–[23] have made every effort to increase the performance of heat transfer. With the intention of increasing the heat transfer and improving the heat exchanger performance, the new idea of simultaneous approach in crossflow heat exchangers is considered for the automotive applications. In automotive, vehicles need appropriate thermal management systems. Radiator is employed in engine cooling systems, and transmission oil cooler to remove excessive heat from the transmission systems. Vehicles use massive amount of fuels to generate operating power. Vehicle performance is usually assessed with regard to the fuel consumption and emissions. The firm emission regulations fixed by the Environmental Protection Agency (EPA) [24] can be mitigated by improving efficiency of power train and thermal performance of heat exchangers in HVAC and engine cooling systems.

The transmission oil cooler is generally sited in front of the radiator in a sequential arrangement. In this pattern, transmission oil cooler releases heat to the ambient air, which gets warmer before entering the radiator. As a result, the heat transfer performance of the radiator becomes lower compared to the condition when the radiator receives fresh ambient ram air. The heat transfer performance of the radiator can be enhanced by transforming the orientation of the heat exchangers.

In this current research, the transmission oil cooler and the radiator are proposed to place in a simultaneous orientation, where both heat exchangers will receive identical ram or incoming air with the similar ambient conditions. The proposed simultaneous heat exchanger module can significantly minimize the operational energy requirements in automotive applications. It can also improve life cycle climate performance (LCCP) and fulfil the strict emission regulations established by the EPA.

Nomenclature

3D	Three dimensional
ATF	Automatic transmission fluid
C	Constant
c_p	Fluid specific heat [J/kgK]
d_h	Hydraulic diameter [m]
EG	50:50 ethylene glycol-water mixture
G	Mass flux [kg/m ² s], constant
HX	Heat exchanger
k	Thermal conductivity [W/mK]
	Turbulence kinetic energy [m ² / s ²]
k_{eff}	Effective thermal conductivity [W/mK]
\dot{m}	Mass flow rate [kg/s]
Pr	Prandtl number
\dot{Q}	Heat transfer rate [w]
Re	Reynolds number
T	Temperature [°C]
u'	Ratio of the r.m.s. of the velocity fluctuations
u_{ave}	Mean velocity of the fluid flow [m/s]

Greek letters

Δ	Change in variable
ρ	Density [kg/m ³]
μ	Dynamic viscosity [kg/m. s or N. s/m ²]
ε	Kinetic energy dissipation rate [m ² /s ³]

Subscripts

a	Air
atf	Automatic transmission fluid
eff	Effective
eg	50:50 ethylene glycol-water mixture
h	Hydraulic
i	Inlet
k	Turbulence kinetic energy
m	Mean, mass weighted average
o	Outlet
s	Channel inner surface
seq	Sequential
sim	Simultaneous
t	Turbulent

2. Numerical Methodology

Numerical simulations of the 3D heat transfer have been conducted through air-to-liquid crossflow heat exchangers using ANSYS Fluent, a widely used finite volume method (FVM) commercial software. Details are illustrated below.

2. 1. Computational Domains

The conventional sequential and simultaneous heat exchanger modules used in this study are presented in Figures 1(a) and 1(b), respectively. The specifications of the HX modules are illustrated in Table 1. The both modules are identical in height, frontal area, and volume. Each domain includes three continuums, ATF, EG and air, with the solid heat exchangers. The air-side has been selected in consideration of the test chamber equipped in the experimental setup.

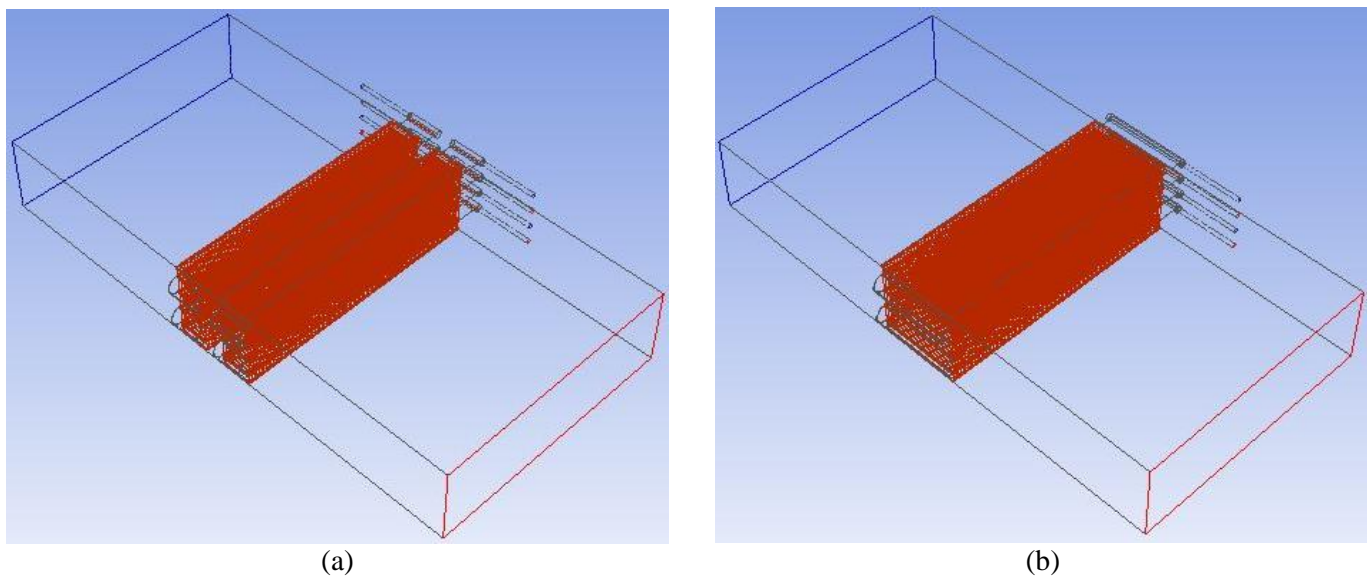


Fig. 1: Computational domains of the crossflow HXs in (a) simultaneous and (b) sequential orientation.

Table 1: Specifications of the heat exchanger modules.

Parameters	Sequential HX	Simultaneous HX	Parameters	Sequential HX	Simultaneous HX
Tube height	1 mm	1 mm	No. of loops	4	2
Gap between HXs	24 mm	-	Slabs in each loop	2	2
Slab width, x	38 mm x 2	100 mm	Fin density	12 per 25.4mm	12 per 25.4mm
Slab thickness, y	2 mm	2 mm	Fin height	16 mm	16 mm
Slab length, z	305 mm	305 mm	Fin thickness	0.1 mm	0.1 mm
Module height	92 mm	92 mm	Inlet/exit tube dia.	4.76 mm	4.76 mm

2. 2. Mesh Generation

Gambit 2.4.6 has been used to generate meshes for each geometry to be applicable for CFD simulations. The whole domain has been divided into several sub-domains that include air, liquid (pipes, manifolds, serpentine, and tubes), and solid (fins and slabs). Each sub-domain has been discretized with the unstructured (T-Grid, tetrahedral, wedge, etc.) cells. The flow passages adjacent to the walls have been carefully clustered and a grid independency study has been carried out to attain the high-quality CFD result. Total number of grid cells used in CFD simulations of sequential module and simultaneous module are 12.49×10^6 and 5.78×10^6 , respectively. Some grids are illustrated in Figures 2(a) and 2(b).

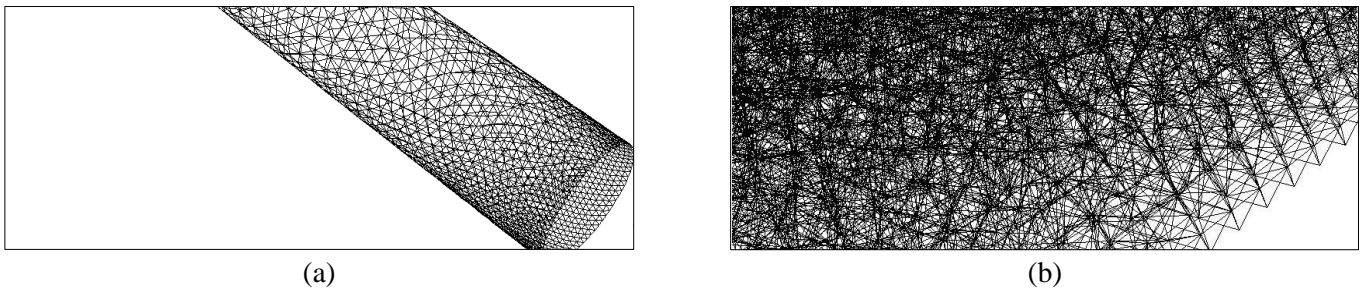


Fig. 2: (a) inlet/outlet pipe mesh (zoomed) and (b) air mesh (zoomed).

2. 3. Assumptions

Following assumptions have been made for the flow geometry and boundary conditions in the current study.

- Single phase incompressible fluids
- Thermophysical properties of air and aluminum are constant; but ATF and EG are temperature dependent
- Adiabatic walls (test chamber, serpentine, manifolds, and tubes); no heat loss or gain to or from the surroundings
- No diffusion or radiation heat transfer in the system

2. 4. Flow Regime

The flow regime of both the ATF and the EG in the flat tubes are laminar; however, the flow of the working fluids, including air in the test chamber as well as ATF and EG in the inlet and outlet pipes are turbulent. For instance, Reynolds numbers (Re) of working fluids at the HX core are $30 \leq Re_{atf,core} \leq 250$, $225 \leq Re_{eg,core} \leq 1900$, and $Re_{a,core} = 6.8 \times 10^4$ and at the inlet boundary are $300 \leq Re_{atf} \leq 4165$; $2375 \leq Re_{eg} \leq 3.3 \times 10^4$, and $Re_{a,i} = 6.1 \times 10^4$.

2. 5. Governing Equations

Based on the key assumptions, the following governing equations have been solved by using ANSYS FLUENT.

Continuity or mass conservation:

$$\frac{\partial}{\partial x_i} (\rho u_i) = 0 \quad (1)$$

Momentum conservation:

$$\frac{\partial}{\partial j} (\rho u_i u_j) = \frac{\partial}{\partial x_j} \left(\mu \frac{\partial u_j}{\partial x_i} \right) - \frac{\partial P}{\partial x_i} + \frac{\partial}{\partial x_j} (-\rho \overline{u_i' u_j'}) \quad (2)$$

Energy conservation:
$$\frac{\partial}{\partial x_i} (\rho u_i T) = \frac{\partial}{\partial x_j} \left(k_{\text{eff}} \frac{\partial T}{\partial x_j} + u_i (\tau_{ij})_{\text{eff}} \right) \quad (3)$$

Turbulence kinetic energy, k:
$$\frac{\partial}{\partial x_i} (\rho k u_i) = \frac{\partial}{\partial x_j} \left[\left(\mu + \frac{\mu_t}{\sigma_k} \right) \frac{\partial k}{\partial x_j} \right] + G_k - \rho \epsilon \quad (4)$$

Turbulence energy dissipation, ϵ :
$$\frac{\partial}{\partial x_i} (\rho \epsilon u_i) = \frac{\partial}{\partial x_j} \left[\left(\mu + \frac{\mu_t}{\sigma_\epsilon} \right) \frac{\partial \epsilon}{\partial x_j} \right] + C_{1\epsilon} \frac{\epsilon}{k} G_k - C_{2\epsilon} \rho \frac{\epsilon^2}{k} \quad (5)$$

where, effective thermal conductivity, $k_{\text{eff}} = k + (C_p \mu_t / \text{Pr}_t)$, deviatoric stress tensor, $(\tau_{ij})_{\text{eff}} = \mu_{\text{eff}} \left((\partial u_j / \partial x_i) + (\partial u_i / \partial x_j) \right) - \frac{2}{3} \mu_{\text{eff}} \left((\partial u_k / \partial x_k) \delta_{ij} \right)$, turbulent viscosity, $\mu_t = \rho C_\mu (k^2 / \epsilon)$, term, $G_k = -\rho \overline{u'_i u'_j} (\partial u_i / \partial x_j)$, Pr_t is the turbulent Prandtl number, $C_{1\epsilon}$, $C_{2\epsilon}$, $C_{3\epsilon}$, and C_μ are constants, and σ_ϵ is turbulent Prandtl number for ϵ .

2. 6. Computational Setup

Model: A 3DDP pressure-based velocity coupling steady state realizable k- ϵ turbulence model with enhanced wall treatment is used to capture the turbulence parameters in thermal and flow fields developed around the air-to-liquid crossflow heat exchanger.

Properties of Fluids: The temperature dependent thermophysical properties of ATF and EG have been used from SAE Technical Paper 902148 [25], Anton-Paar Instruments [26], Fluid Properties Calculator [27], and CAN-AM Instruments Ltd. [28].

Solution Methods: SIMPLE algorithm is used with the spatial discretization of Least Square Cell Based gradient, Standard Pressure, and Second Order Upwind energy schemes.

Residuals: The consecutive iteration has been stopped when the normalized absolute residuals in each control volume for the flow and the energy variables have been reduced to 10^{-3} and 10^{-9} , respectively.

Turbulence intensity: The turbulence intensity, I is computed as $I = \frac{u'}{u_{\text{ave}}} = 0.16 \text{Re}_{d_h}^{-1/8}$.

where, Re_{d_h} , u' , and u_{ave} are the Reynolds number of fluid based on hydraulic diameter (d_h), the ratio of the root-mean-square of the velocity fluctuations, and the mean velocity of fluid flow.

2. 7. Boundary conditions

Following boundary conditions have been applied in the current study:

- Inlet ATF and EG: mass flow rates and temperature are applied
- Inlet air: velocity and temperature are applied
- Outlet ATF, EG, and air: Pressure outlet boundary condition is applied.
- Walls (test chamber, tubes, manifolds, and serpentine): No slip, stationary, and adiabatic conditions are applied

2. 8. Evaluation of Heat Transfer Rate

The heat transfer rate (\dot{Q}), and the enhancement of heat transfer rate enhancement (Q_{enh}) have been evaluated as

$$\dot{Q} = \dot{m} C_p \Delta T \quad (6)$$

$$Q_{\text{enh}} [\%] = (\dot{Q}_{\text{sim}} / \dot{Q}_{\text{seq}}) \times 100 \quad (7)$$

where c_p = fluid specific heat, \dot{m} = mass flow rate, and ΔT = temperature difference between fluid inlet and outlet. The subscripts *sim* and *seq* represent simultaneous and sequential arrangements, respectively.

3. Results and Discussions

In this section, the predictions of sequential and simultaneous modules of heat exchangers are presented. Both modules are identical in slab thickness, frontal area and volume. Automatic transmission fluid (ATF) with inlet

temperatures of 150°C and 50% ethylene glycol-water mixture (EG) with inlet temperature of 105°C have been cooled by crossflow air with inlet temperature of 25°C and velocity of 6.3m/s. The mass fluxes of both liquids have been varied from 130 kg/m²s to 615 kg/m²s. For sequential module, two possible situations have been considered. In Case-I, the EG-HX has been employed in front of the ATF-HX with regard to the incoming ambient air. While, in Case-II, the ATF-HX has been placed in forward-facing with respect to the ram air. In simultaneous module, the ATF-HX has been positioned on the top of the EG-HX. The boundary conditions of each model has been chosen in consideration of the operating conditions of an automotive transmission cooler and radiator when the vehicle runs in the city during the fall.

3. 1. Case-I: Sequential Heat Exchanger (HX) Module vs Simultaneous HX Module

In this section, heat transfer rates of sequential and simultaneous modules for Case-I are illustrated. Figures 3(a) and 3(b) represent the heat transfer rate of ATF-HX and EG-HX, respectively. The heat transfer rate (\dot{Q}) increases with the increase of Reynolds number, as expected. Figure 3(a) displays about 23% to 25% elevated \dot{Q} of the ATF-HX in simultaneous orientation than the sequential orientation. This is because, the ATF-HX gets the upcoming ambient air in simultaneous module, while it receives the outlet warmer air of EG-HX in case of sequential. Figure 3(b) shows a little enhanced \dot{Q} in simultaneous arrangement at $Re \approx 800$ and gradually becomes insignificant or somewhat lower than that of the sequential at $Re \geq 800$. This is because, at this point, the outlet temperature of ATF supersedes the inlet temperature of EG, i.e. 105°C as shown in Figure 4. Another reason is the thermal interaction between ATF-EX and EG-HX in simultaneous module. The inlet slab of EG-HX and the outlet slab of ATF-HX are connected by fins and transfer heat through the fins.

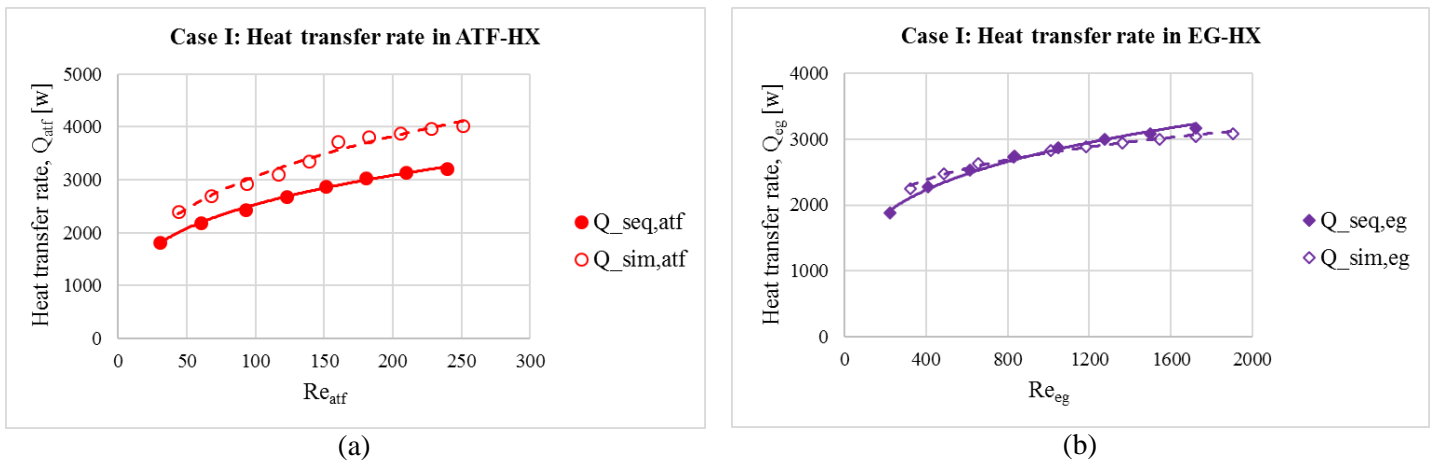


Fig. 3: Heat transfer rate of (a) ATF-HX and (b) EG-HX in simultaneous and sequential modules for Case-I.

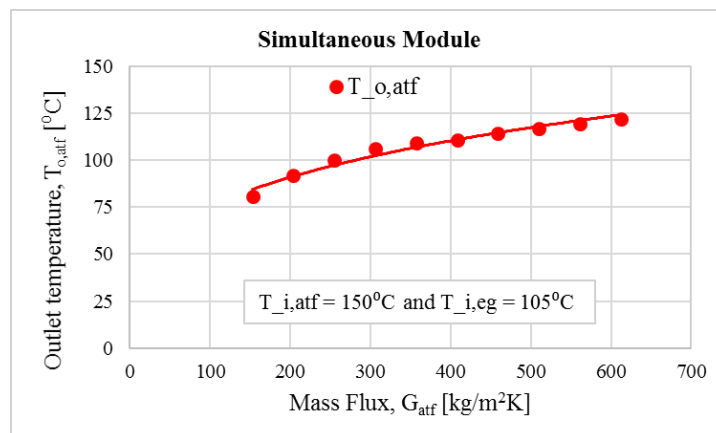


Fig. 4: ATF outlet temperature in simultaneous heat exchanger module.

The overall heat transfer rate in simultaneous and sequential modules are illustrated in Figures 5(a). It is clear from the figure 5(a) that at a given Reynolds number, the overall heat transfer performance of simultaneous HX is better than that of the conventional sequential HX. The total heat transfer rate in simultaneous HX is found to be about 10% to 18% higher than that of the sequential HX as shown in Figure 5(b).

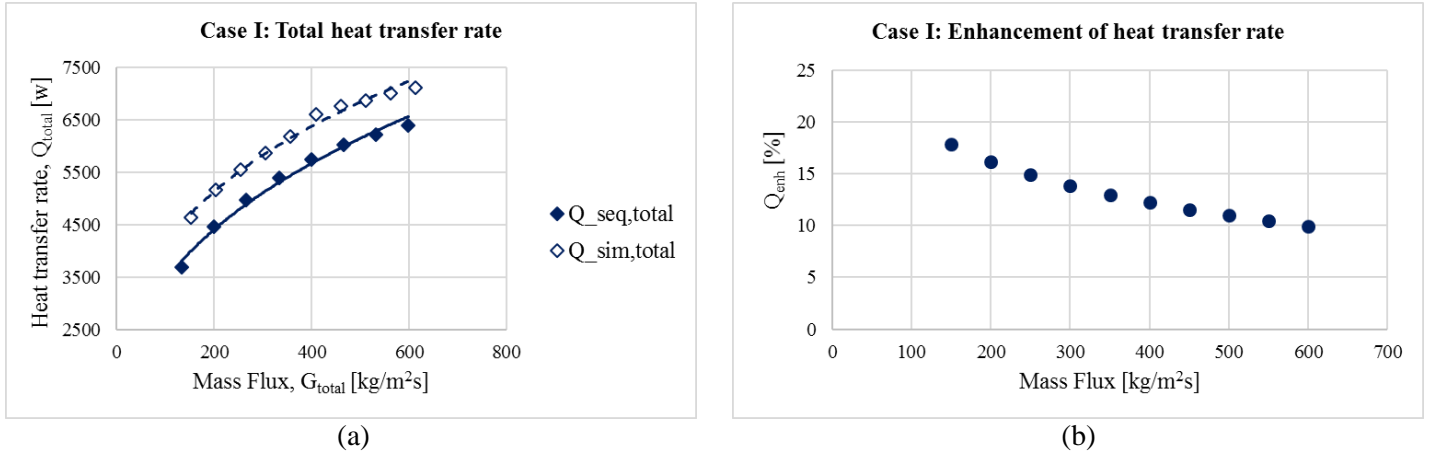


Fig. 5: (a) Overall heat transfer rate in simultaneous and sequential HXs and (b) heat transfer enhancement for Case-I.

3. 2. Case II: Sequential HX Module vs Simultaneous HX Module

Heat transfer rates of simultaneous and sequential HX modules for Case-II are presented in this section. Figure 6(a) illustrates the heat transfer rate of EG-HX which has been placed behind the ATF-HX with regard to the incoming ambient air. The figure shows significant improvement of heat transfer rate in simultaneous module than the sequential orientation. The enhancement of heat transfer rate in simultaneous arrangement is predicted to be about 24% to 29% compared to the conventional sequential one. This is because, in simultaneous situation, the EX-HX gets the fresh incoming ambient air, while it receives warmer outgoing air of the ATF-HX in case of sequential arrangement.

Figure 6(b) represents the heat transfer rate of ATF-HX which has been placed in front of the EG-HX with regard to the incoming ambient cold air. As expected, the heat transfer rate increases with increase of Reynolds number. About 7% to 12% improvement in heat transfer rate of the ATF-HX has been observed in simultaneous orientation than the conventional sequential arrangement. This is because, both the ATF-HX and EG-HX get the incoming ambient air in simultaneous arrangement, while the EG-HX receives delivery of the outlet warmer air of the ATF-HX in sequential module. There is also thermal interaction between ATF-EX and EG-HX in simultaneous arrangement. The inlet slab of EG-HX and the outlet slab of ATF-HX are connected by fins and transfer heat by means of thermal interaction.

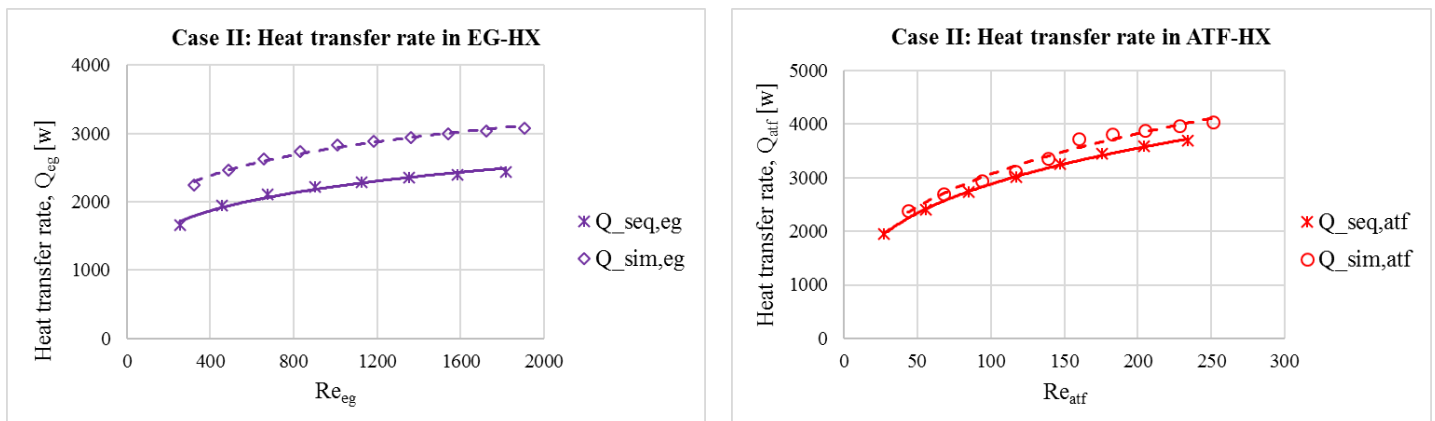


Fig. 6: Heat transfer rate of (a) EG-HX and (b) ATF-HX in simultaneous and sequential modules for Case-II.

The inlet temperature of EG is 105°C for both the simultaneous and the sequential modules. On the other hand, the outlet temperature of ATF temperature varies from 80°C to 120°C , which has shown earlier in Figure 4. The overall heat transfer rate in simultaneous and sequential heat exchangers are illustrated in Figure 7(a). The total heat transfer rate of simultaneous HX is better than that of the conventional sequential HX. The heat transfer rate in simultaneous HX is found to be about 14% to 20% higher than that of the sequential HX as shown in Figure 7(b).

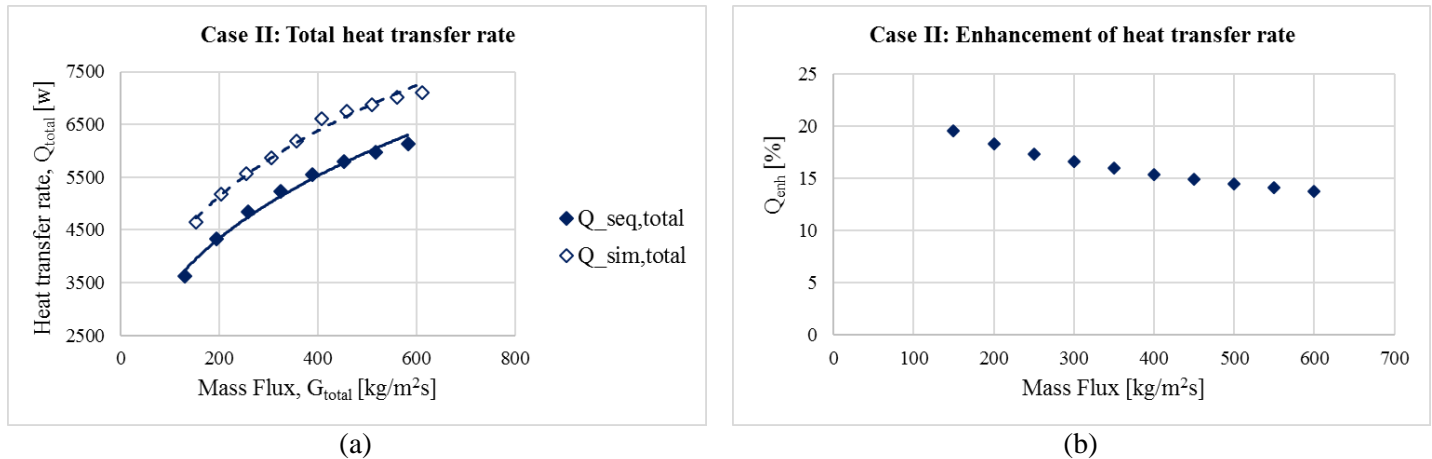


Fig. 7: (a) Overall heat transfer rate in simultaneous and sequential modules and (b) heat transfer enhancement for Case-II.

4. Conclusion

The current study has been conducted to achieve numerical investigation of heat transfer in sequential and simultaneous heat exchanger modules. The following conclusions have been drawn from the research findings:

- Simultaneous heat exchanger module outperforms conventional sequential module.
- The enhancement in heat transfer rate has been predicted to be about 24% to 29% for EG-HX and 7% to 12% for ATF-HX due to the replacement of sequential arrangement with the simultaneous module. The overall enhancement has been found to be 14% to 20%.
- The proposed simultaneous module, where both HXs will receive identical incoming cold air with the similar ambient conditions can significantly improve the heat transfer performance.
- It can reduce the operational energy requirements in heat exchanger applications, especially in automotive HVAC and cooling systems. It can also enhance the life cycle climate performance (LCCP) and fulfil the emission standards set by the EPA.

Acknowledgements

The authors gratefully acknowledge the Natural Sciences and Engineering Research Council of Canada (NSERC) for providing discovery grant (DG) to accomplish the current research. The authors are also thankful to the department of Mechanical Automotive & Materials Engineering at University of Windsor for giving the Postdoctoral research opportunity.

References

- [1] M. G. Khan and A. Fartaj, "A review on microchannel heat exchangers and potential applications," *Int. J. Energy Res.*, vol. 35, pp. 553–582, 2011.
- [2] J. Liu, S. Hussain, W. Wang, L. Wang, G. Xie, and B. Sundén, "Heat transfer enhancement and turbulent flow in a rectangular channel using perforated ribs with inclined holes," *J. Heat Transfer*, vol. 141, pp. 041702, 1–15, 2019.
- [3] E. S. Dasgupta, S. Askar, M. Ismail, A. Fartaj, and M. A. Quaiyum, "Air cooling by multiport slabs heat exchanger: An experimental approach," *Exp. Therm. Fluid Sci.*, vol. 42, pp. 46–54, 2012.
- [4] M. Ismail, A. Fartaj, and M. Karimi, "Numerical investigation on heat transfer and fluid flow behaviors of viscous fluids in a minichannel heat exchanger," *Numer. Heat Transf. Part A Appl.*, vol. 64, no. 1, pp. 1–29, 2013.
- [5] S. Fotowat, A. Fartaj, M. Ismail, M. A. Quaiyum, and S. Askar, "Experimental study on air-heating through a cross-

- flow minichannel heat exchanger,” *CSME Bienn. Int. Conf.*, pp. 1–6, 2012.
- [6] M. A. Quaiyum, M. Ismail, and A. Fartaj, “Study of automatic transmission fluid in a serpentine minichannel heat exchanger: An experimental approach,” *Exp. Heat Transf.*, vol. 28, no. 3, pp. 244–266, 2015.
- [7] W. Wang and X. Wang, “Experiments of condensation heat transfer in micro channel heat exchanger,” in *International Refrigeration and Air Conditioning Conference at Purdue*, 2010, pp. 2290, 1–6.
- [8] A. Arteconi, G. Giuliani, M. Tartuferi, and F. Polonara, “Characterization of a mini-channel heat exchanger for a heat pump system,” *J. Phys. Conf. Ser.*, vol. 501, no. 1, pp. 0–10, 2014.
- [9] M. Asadi, G. Xie, and B. Sunden, “A review of heat transfer and pressure drop characteristics of single and two-phase microchannels,” *Int. J. Heat Mass Transf.*, vol. 79, pp. 34–53, 2014.
- [10] Y. Zhai, G. Xia, Z. Li, and H. Wang, “Experimental investigation and empirical correlations of single and laminar convective heat transfer in microchannel heat sinks,” *Exp. Therm. Fluid Sci.*, vol. 83, pp. 207–214, 2017.
- [11] Z. Li, W. Q. Tao, and Y. L. He, “A numerical study of laminar convective heat transfer in microchannel with non-circular cross-section,” *Int. J. Therm. Sci.*, vol. 45, pp. 1140–1148, 2006.
- [12] E. S. Dasgupta, F. A. Siddiqui, and A. Fartaj, “Experimental study on air side heat transfer and fluid flow characteristics of microchannel heat exchanger,” *SAE Int. J. Mater. Manuf.*, vol. 4, no. 1, pp. 1198–1210, 2012.
- [13] M. Ismail, S. Fotowat, and A. Fartaj, “Effect of channel size on heat transfer and pressure drop in thin slabs minichannel heat exchanger,” *Int. J. Mech. Eng. Mechatronics*, vol. 2, no. 1, pp. 32–41, 2014.
- [14] A. Jokar, S. J. Eckels, and M. H. Hosni, “Single-phase flow in meso-channel compact heat exchangers for air conditioning applications,” *Heat Transf. Eng.*, vol. 31, no. 1, pp. 3–16, 2010.
- [15] S. G. Kandlikar, “Fundamental issues related to flow boiling in minichannels and microchannels,” *Exp. Therm. Fluid Sci.*, vol. 26, no. 2–4, pp. 389–407, 2002.
- [16] S. G. Kandlikar, “A roadmap for implementing minichannels in refrigeration and air-conditioning systems - Current status and future directions,” *Heat Transf. Eng.*, vol. 28, no. 12, pp. 973–985, 2007.
- [17] M. S. Saadi, M. Ismail, S. Fotowat, M. A. Quaiyum, and A. Fartaj, “Study of motor oil cooling at low Reynolds number in multi-port narrow channels,” *SAE Int. J. Engines*, vol. 6, no. 2, pp. 1287–1298, 2013.
- [18] M. A. Quaiyum, A. Fartaj, and S. Askar, “An experimental characterization of automatic transmission fluid flowing through air cooled microchannel heat exchanger,” *SAE Int. J. Mater. Manf.*, vol. 5, no. 2, pp. 503–516, 2012.
- [19] Y. Fan and L. Luo, “Recent applications of advances in microchannel heat exchangers and multi-scale design optimization,” *Heat Transf. Eng.*, vol. 29, pp. 461–474, 2008.
- [20] S. Kandlikar, “Effect of liquid-vapor phase distribution on the heat transfer mechanisms during flow boiling in minichannels and microchannels,” *Heat Transf. Eng.*, vol. 27, no. 1, pp. 4–13, 2006.
- [21] M. G. Khan, “Experimental investigation of heat transfer and pressure drop characteristics of water and glycol-water mixture in multi-port serpentine microchannel slab heat exchangers,” Ph.D. dissertation, Dept. Mech. Auto. Mat. Eng., Univ. Windsor, ON, Canada, 2011.
- [22] N. B. Chien, P. Q. Vu, N. M-Ghazali, and O. J-Taek, “Convective heat transfer characteristics of single phase liquid in multiport minichannel tube: Experiment and CFD simulation,” *Energy Procedia*, vol. 75, pp. 3180–3185, 2015.
- [23] M. E. Steinke and S. G. Kandlikar, “Single-phase heat transfer enhancement techniques in microchannel and minichannel flows,” in *The 2nd International Conference on Microchannels and Minichannels*, 2004, pp. 1–8.
- [24] EPA, “Emission standards reference guide for on-road and nonroad vehicles and engines,” *U.S. Environmental Protection Agency*, 2016.
- [25] S. P. Kemp and J. L. Linden, “Physical and Chemical Properties of a Typical Automatic Transmission Fluid,” in *SAE International in United States*, 1990, p. Technical Paper 902148.
- [26] “Viscosity of Automatic Transmission fluid (ATF) – viscosity table and viscosity chart.” [Online]. Available: <https://wiki.anton-paar.com/en/automatic-transmission-fluid-atf/>
- [27] “Fluid Properties Calculator, Microelectronics Heat Transfer Laboratory, University of Waterloo.” [Online]. Available: <http://www.mhtl.uwaterloo.ca/old/onlinetools/airprop/airprop.html>.
- [28] “CAN-AM Instruments Ltd., 2851 Brighton Road, Oakville, Ontario, L6H 6C9, Canada.”